J. Fluid Mech. (1973), *vol.* 58, *part* 2, *pp.* 389–402
Printed in Great Britain

The interaction of two opposing plane turbulent wall jets

By R. J. KIND AND K. SUTHANTHIRAN
Division of Aerothermodynamics, Carleton University, Ottawa

(Received 16 March 1972)

An experimental study was made of the interaction produced by the collision, in still air, of two diametrically opposed plane turbulent wall jets. Distributions of time-average velocity, longitudinal turbulence and static pressure on the wall were measured. Simple universal relations giving the position of interaction and the maximum wall static pressure are deduced from the measurements and are explained in terms of the 'frozen-flow' concept. There is little or no loss of momentum due to mixing in the interaction process. The free jet that results from the interaction has the same velocity distribution as a conventionally generated two-dimensional free jet, but its rate of spread and turbulence level are about three times larger.

1. Introduction

This paper describes an experimental investigation of the interaction which occurs when a two-dimensional turbulent wall jet in still air meets another such wall jet flowing in the opposite direction. The flow is sketched in figure 1. After the two wall jets collide the combined flow must proceed away from the wall as sketched; this re-direction of the flow requires that the wall static pressure in the interaction region be greater than the ambient static pressure. Thus each wall jet sees an adverse pressure gradient along the wall as it enters the interaction region and as a result it separates from the wall. A separation bubble therefore exists in the interaction region, as shown in figure 1.

This flow is of interest in connexion with the use of tangential blowing to control the circulation around aerofoils having bluff trailing edges as described, for example, by Kind (1967) or Kind & Maull (1968). The flow over such an aerofoil, with blowing from one slot only, is sketched in figure 2. The separation bubble shown in figure 2 could be suppressed by blowing relatively weakly from a suitably located slot in the lower surface of the aerofoil and it is thought that this might considerably reduce mixing losses and thus improve the drag performance of the aerofoil. In such cases the wall jet issuing from the main blowing slot on the upper surface would meet the wall jet from the lower-surface slot at some point around the trailing edge, giving rise to a somewhat more complex version of the flow studied in the present investigation. Information about the position of the interaction, the direction of the jet after the interaction and the momentum loss due to the interaction would be of interest with respect to this application since

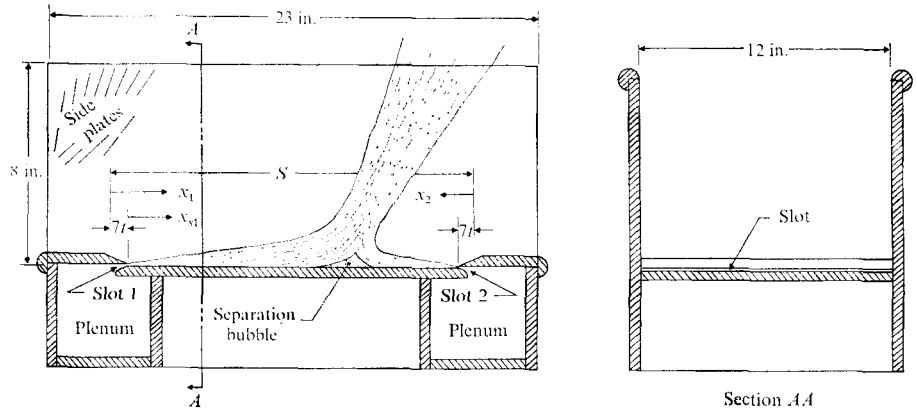

FIGURE 1. Sketch of apparatus and flow.

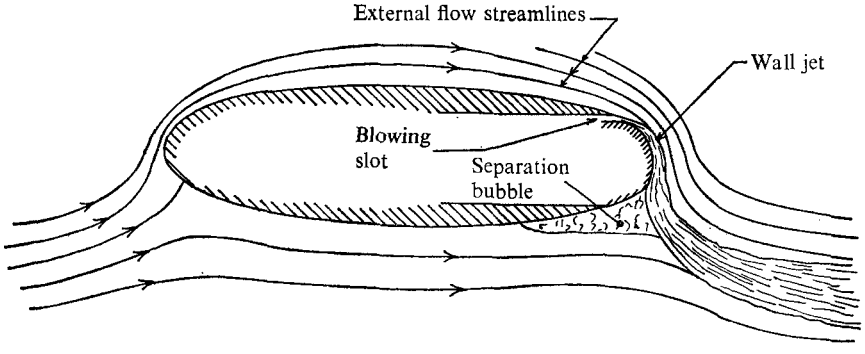

FIGURE 2. Flow over a bluff body with circulation control.

these factors would have an important influence on the lift and drag of the aerofoil.

The present flow might also form the basis of a new type of fluidic proportional amplifier. It is also of considerable interest in its own right.

2. Experimental arrangement and procedure

Figure 1 shows a cross-section of the apparatus used in the present work and also shows some of the nomenclature. The distance between the blowing slots was 15 in. and the width of the apparatus was 12 in. Side plates were present to aid in maintaining two-dimensional flow conditions. The nominal slot thickness t was $\frac{1}{16}$ in. and the slot thickness was uniform to within $\pm 0{\cdot}8\,\%$. The flow from the slots discharged tangentially to a flat polished steel plate along whose centre-line 61 static-pressure tappings ($\frac{1}{64}$ in. in diameter) were present. Each plenum chamber was fed from both sides by a variable-speed centrifugal blower unit; the mass flow rates were measured by means of orifice-plate flowmeters. The mean velocity of the flow from the slots was determined by assuming frictionless expansion from the measured stagnation pressures in the plenum chamber with a small correction

for the boundary layers on the nozzle walls. Time-average velocity and longitudinal turbulent intensity were measured using a linearized constant-temperature hot-wire anemometer unit with, unless otherwise mentioned, a DISA type 55A25 probe operating at an overheat ratio of 2; the fluctuating portion of the signal from the anemometer unit was measured by a true r.m.s. voltmeter.

The flow was checked for two-dimensionality by using surface flow visualization on the wall and by measuring velocity profiles and skin friction (with a Preston tube) at various spanwise positions. The surface flow visualization showed that the limiting streamlines were straight and parallel and that the separation lines were straight and perpendicular to the direction of the flow. The Preston tube readings and the maximum velocity, thickness and shape of the velocity profiles were found to be invariant with spanwise position, except of course near the side plates of the apparatus.

The experimental programme consisted of measurements of time-average streamwise velocity profiles and profiles of the longitudinal component of the turbulent velocity fluctuations throughout the flow for various values of J_1/J_2, the ratio of the wall-jet momentum fluxes at the slots. The static-pressure distributions along the wall were also measured. The Reynolds number $U_J t/\nu$ ranged between $4{\cdot}8 \times 10^3$ and 8×10^3, with $6{\cdot}5 \times 10^3$ being used for the strong jet in most runs; U_J is the mean velocity of the jet at the slot exit. No significant Reynolds-number effects were observed.

3. Experimental results

Figure 3 is a non-dimensional plot of wall-jet velocity profiles measured outside the interaction region under a variety of conditions. The local maximum velocity U_m and the local half-velocity thickness $y_{\frac{1}{2}m}$ serve as the normalizing parameters in figure 3; $y_{\frac{1}{2}m}$ is the value of y, the co-ordinate normal to the wall, at which the local velocity $U = \frac{1}{2}U_m$. The excellent collapse of the results is noteworthy. These and other velocity-profile measurements were used to obtain the rates of growth and decay of the wall-jet thickness $y_{\frac{1}{2}m}$ and of the maximum velocity U_m, respectively; these results are presented in figures 4 (*a*) and (*b*). From figure 4 (*a*) it is seen that the virtual origin† of the wall jet is about 7 slot thicknesses upstream of the slot exit.

The wall-jet growth rate obtained from figure 4 (*a*) is

$$dy_{\frac{1}{2}m}/dx = 0{\cdot}081. \tag{1}$$

This growth rate is somewhat larger than the value of about 0·07 found by a number of other investigators (e.g. Gartshore & Newman 1969; Kruka & Eskinazi 1964); on the other hand the present growth rate is in agreement with that found by Giles, Hays & Sawyer (1965) and by Myers, Schauer & Eustis (1963) for a plane still-air wall jet. The cause of the differences in growth rates observed by various investigators is not clear at present. It was found that varying the turbulence level

† The virtual origin is defined as the position at which a slot of infinitesimal thickness emitting the same momentum flux as the real slot would produce the same flow as that actually observed.

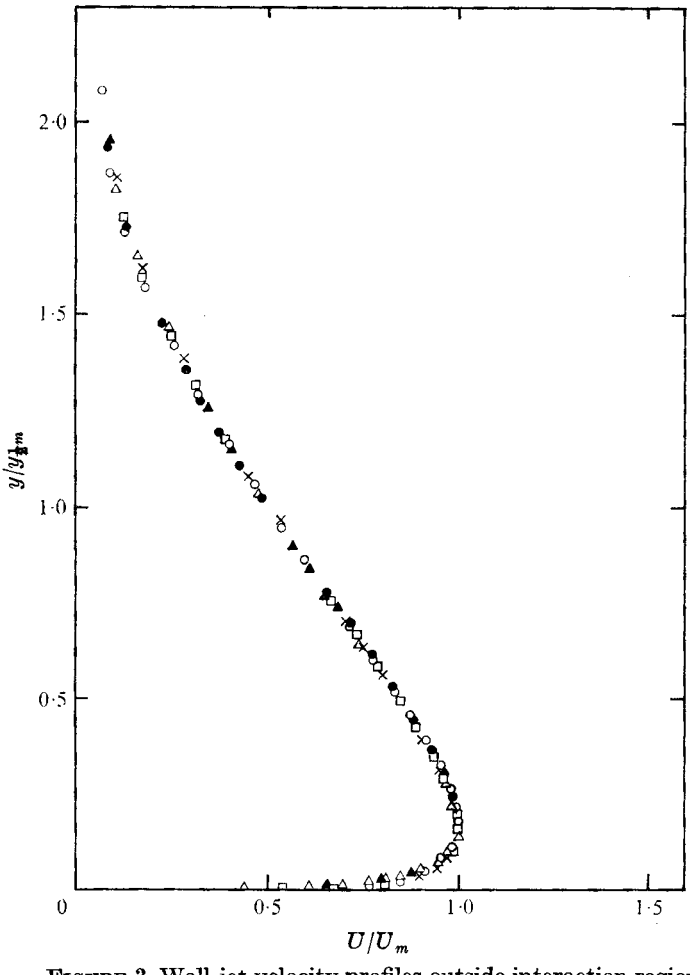

FIGURE 3. Wall-jet velocity profiles outside interaction region.

	○	□	●	×	△	▲
x_{s1}/t	39	156	17	80	111	49
J_1/J_2	∞	∞	0·95	0·95	∞	0·95
$(U_{J_1}t/\nu)\times 10^{-3}$	6·5	6·5	6·5	6·5	4·8	4·8

of the flow issuing from the blowing slots from 0·3 % to 2 % had no significant effect on the growth rate; varying the temperature difference between the blowing air and ambient air from 5 to 30 °F also had no significant effect. In any case the findings of the present investigation with respect to the interaction process should be valid regardless of the growth rate of the wall jets that are involved.

The data of figure 4 (*b*) are closely fitted by the straight line

$$U_m/U_J = 4{\cdot}0(x/t)^{-0.5} - 0{\cdot}04. \tag{2}$$

U_J is the mean velocity at the slot exit and x is the distance downstream of the virtual origin.

Distributions of static pressure along the wall for various values of J_1/J_2 are

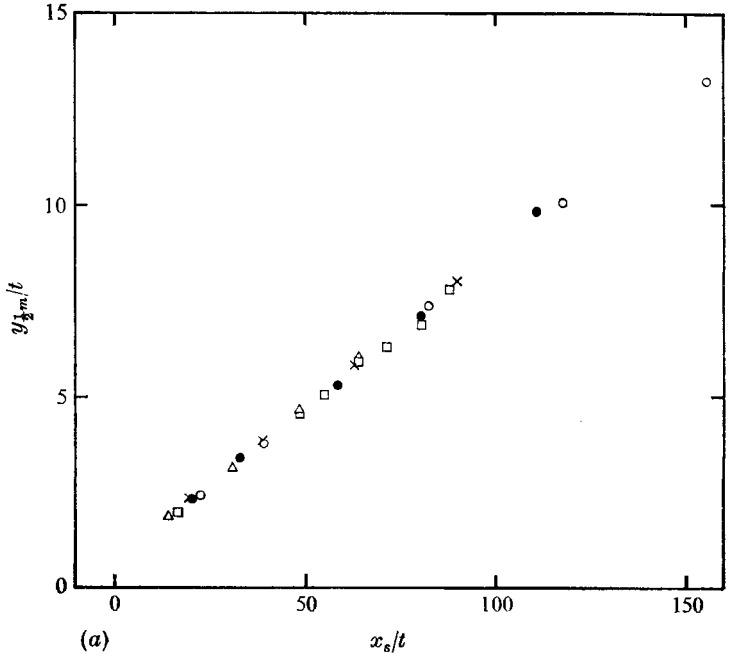

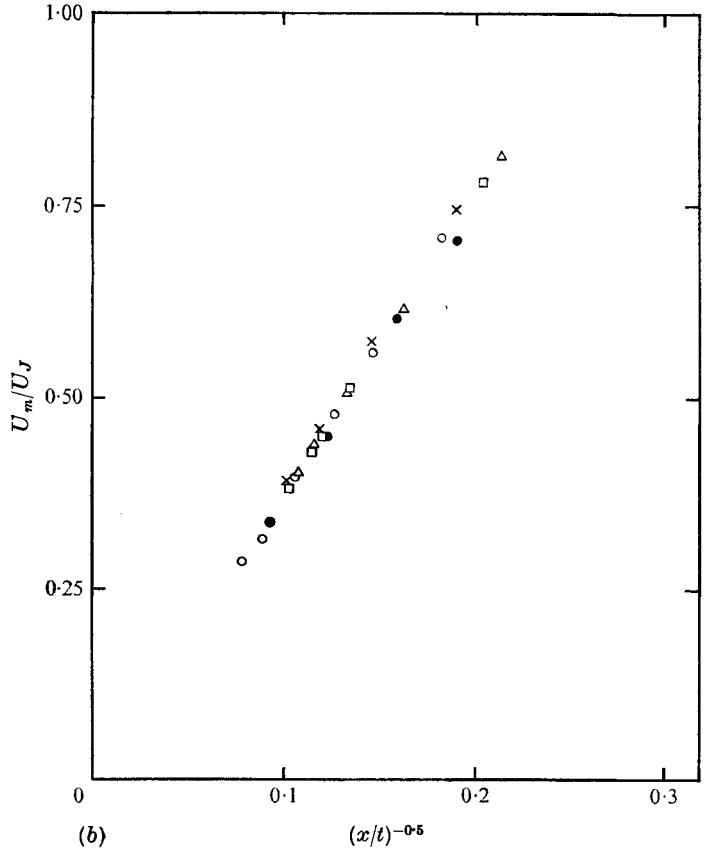

FIGURE 4. (*a*) Wall-jet growth and (*b*) wall-jet maximum-velocity plot.

	○	□	●	△	×
J_1/J_2	∞	0·95	∞	0·95	0
$(U_J t/\nu) \times 10^{-3}$	6·5	6·5	4·8	4·8	4·8

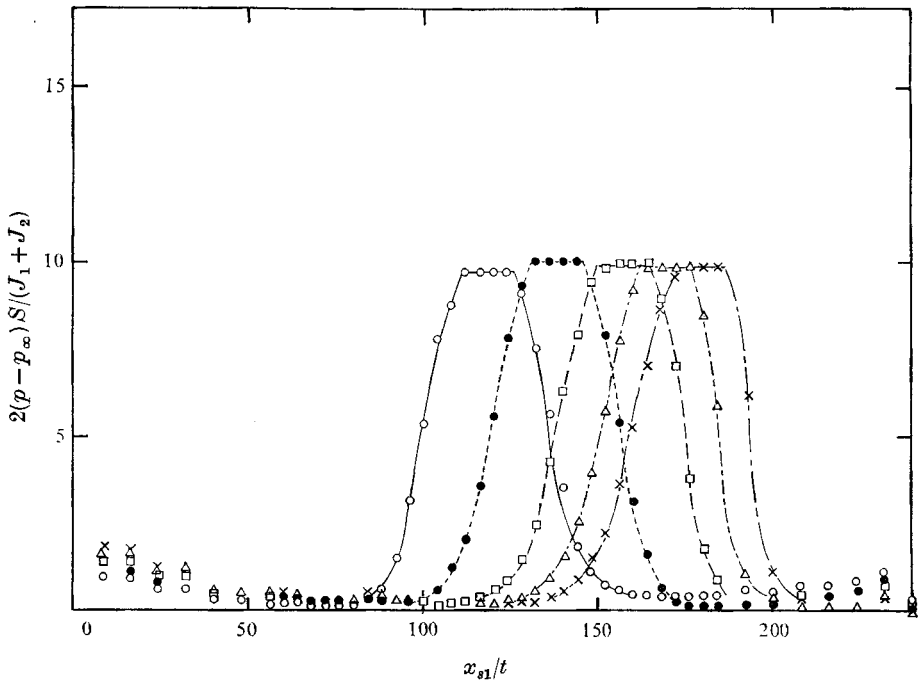

FIGURE 5. Static-pressure distribution along wall. $U_{J_1}t/\nu = 8\times10^3$. ○, $J_1/J_2 = 0{\cdot}95$; ●, 1·42; □, 1·9; △, 2·35; ×, 2·8.

plotted in figure 5. The presence of a separation bubble in the interaction region (as outlined in § 1) is clearly indicated by the region of constant pressure on each of the distributions; the adverse pressure gradient leading to separation is seen to be very steep in all cases. An interesting result that is obvious from figure 5 is that

$$2(p_{\text{sep}}-p_\infty)S/(J_1+J_2) = 9{\cdot}9 \tag{3}$$

for all values of J_1/J_2. S is the distance between the virtual origins of the two wall jets and p_{sep} is the static pressure in the separation bubble.

Let us define the position of the interaction as the midpoint of the region of constant pressure that is observed in the wall-static-pressure distribution. This position will depend on where the two wall jets separate owing to the adverse pressure gradient which is induced along the wall as a result of the interaction process. The separation pressure of both wall jets must of course be the same because the pressure in the separation bubble is constant. It would appear that the position of the interaction would be very difficult to predict analytically since it would involve calculation of wall-jet development and separation in a situation where the boundary-layer equations are not valid and where the static-pressure distribution is not known beforehand. The measurements reveal, however, that a very simple correlation applies; the interaction positions are determined from figure 5 and when plotted as in figure 6 it is obvious that

$$x_{1i}/x_{2i} = J_1/J_2, \tag{4}$$

where x_i denotes the distance from the virtual origin to the position of interaction.

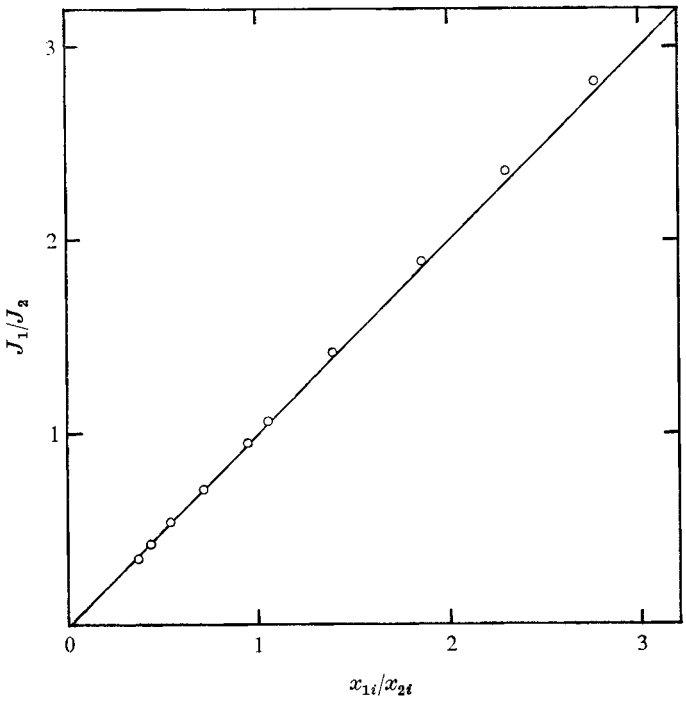

FIGURE 6. Wall-jet momentum ratio *vs.* interaction position ratio.
○, experimental results; ——, equation (4).

The results given by equations (3) and (4) can be generalized by use of the information contained in figures 3 and 4. Since all still-air wall-jet velocity profiles are similar (figure 3) the momentum flux is proportional to the product $U_m^2 y_{\frac{1}{2}m}$. Therefore we can write

$$J' = k\rho U_m^2 y_{\frac{1}{2}m}, \tag{5}$$

where J' is the local momentum flux in the wall jet and k is a constant of proportionality (from figure 3, $k = 0{\cdot}75$). Figure 4(*a*) shows that $y_{\frac{1}{2}m} = 0{\cdot}08x$; equation (5) can therefore be rewritten as

$$J' = 0{\cdot}06\rho U_m^2 x. \tag{6}$$

From the growth law and the maximum-velocity decay law given by (1) and (2) respectively, it follows that downstream of about $x/t = 20$

$$J'/J = 0{\cdot}98 - 0{\cdot}019(x/t)^{0{\cdot}5}. \tag{7}$$

Equation (7) is merely a fit to the experimental data and no deeper significance should be attached to it; in particular, the accuracy of (7) is not such that it would yield a satisfactory skin-friction law if differentiated. By combining (7) with (4) and assuming that $0{\cdot}019[(x_{1i}/t)^{0{\cdot}5} - (x_{2i}/t)^{0{\cdot}5}]$ is much less than unity it can be shown that at the position of interaction

$$U_{m1i}/U_{m2i} \doteqdot 1, \tag{8}$$

where the subscript i denotes the value that the parameter would have at the position of interaction if the other wall jet were absent. Detailed calculations on

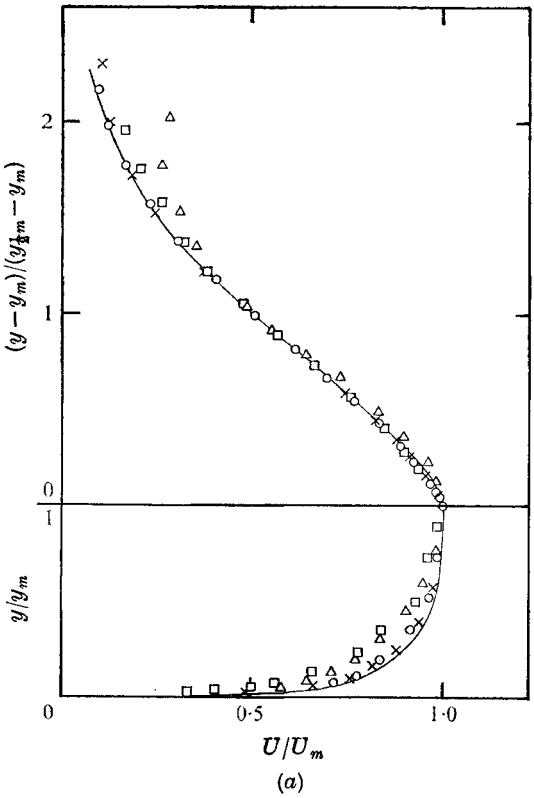

FIGURE 7(a). For legend see facing page.

the present data show this relation to be correct to within about 3 %. Thus the maximum velocity U_{mi} is the same for both wall jets at the interaction position; the thicknesses $y_{\frac{1}{2}m}$ are not, however, equal except for the special case $J_1 = J_2$. Since $x_{1i}+x_{2i} = S$ it follows from (6) and (8) that

$$(J_1'+J_2')_i = 0{\cdot}06\rho U_{mi}^2 S. \tag{9}$$

Using (7) and (4) it can be shown that within the range of the present experiments ($0{\cdot}3 < J_1/J_2 < 3$) the following relation holds to a good approximation at the position of interaction:

$$(J_1'+J_2')_i \doteqdot 0{\cdot}75(J_1+J_2). \tag{10}$$

Substitution from (10) into (9) yields

$$(J_1+J_2) \doteqdot 0{\cdot}08\rho U_{mi}^2 S. \tag{11}$$

Thus (3) can be re-written as

$$(p_{\text{sep}}-P_\infty)/\tfrac{1}{2}\rho U_{mi}^2 \doteqdot 0{\cdot}8. \tag{12}$$

Another useful relation is obtained by substituting for ρU_{mi}^2 from (12) into (5):

$$J_i'/(p_{\text{sep}}-p_\infty)\, y_{\frac{1}{2}mi} \doteqdot 1{\cdot}9. \tag{13}$$

Equations (8), (12) and (13) are not restricted to the present apparatus and should hold regardless of the growth rate of the wall jets because no streamwise distances appear and because the wall-jet velocity-profile shape is essentially the same in all investigations. Comparison of the present velocity profiles with those of Kind (1967) indicates that even strong convex surface curvature does not

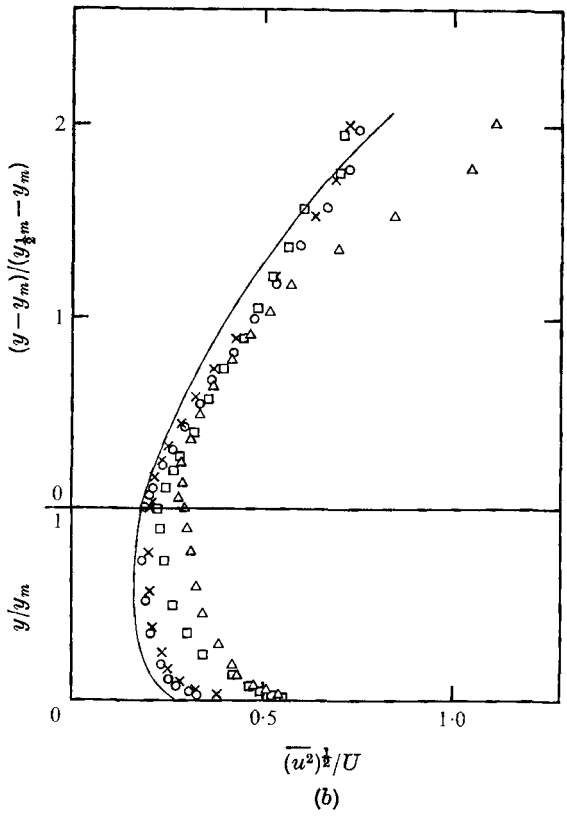

FIGURE 7. (*a*) Wall-jet velocity profiles and (*b*) longitudinal turbulence of wall jet inside interaction region. $U_{J_1}t/\nu = 8\times10^3$; $J_1/J_2 = 1{\cdot}9$. For $2(p-p_\infty)S/(J_1+J_2) \doteqdot 3{\cdot}5$: ○, $x_{s1}/t = 135$; ×, $x_{s1}/t = 177$. For $2(p-p_\infty)S/(J_1+J_2) \doteqdot 6{\cdot}8$: □, $x_{s1}/t = 141$; △, $x_{s1}/t = 172$. ——, mean results for wall jet upstream of interaction. u is the streamwise component of the turbulent fluctuation velocity.

greatly alter the shape of the wall-jet velocity profiles; consequently (8), (12) and (13) should also hold, at least approximately, on curved surfaces and even for wall jets in a moving stream provided that the ratio U_m/U_∞ is reasonably large and that local values are used for the wall-jet momentum flux J'. For example, in the application to circulation-controlled aerofoils that was outlined in §1, the position of the interaction between the two wall jets could be estimated by noting the position at which the calculated values of U_m were the same for both wall jets; a suitable method (e.g. Kind 1971) would, of course, have to be used for calculating the development of the wall jets.

Figures 7 (*a*) and (*b*) present profiles of time-average velocity and longitudinal turbulence measured inside the interaction region, in the adverse pressure gradient before separation. For comparison, measurements taken upstream of the interaction region are included in figures 7 (*a*) and (*b*). Both the shape of the velocity profile and the turbulence level in the inner layer of the wall jets change in the expected way owing to the adverse pressure gradient. It is noteworthy that at a given pressure coefficient (obtained from figure 5) the velocity profiles and the turbulence distributions are, within experimental error, the same in the inner

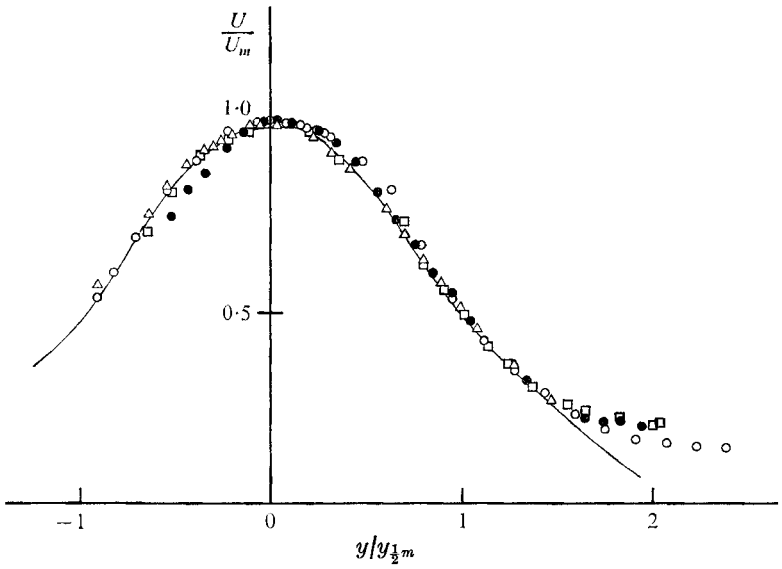

FIGURE 8. Velocity profiles in free jet after interaction. ——, experimental results of Forthmann (1934, see Schlichting 1960) for two-dimensional turbulent free jet. $U_{J_1}t/\nu = 6{\cdot}5 \times 10^3$. For $J_1/J_2 = 0{\cdot}95$: ○, $x_w/(y_{\frac{1}{2}m1i}+y_{\frac{1}{2}m2i}) = 1{\cdot}7$; □, 2·4; ●, 2·93. △, $J_1/J_2 = 1{\cdot}9$; $x_w/(y_{\frac{1}{2}m1i}+y_{\frac{1}{2}m2i}) = 3{\cdot}46$. x_w is the distance from the wall measured along the centre-line of the free jet.

layer of both the weak and the strong wall jets, despite the different thicknesses of the two wall jets. This point will receive further comment in the next section of this paper. It should be noted that, since the pressure gradients in the interaction region are very steep, measurements taken in this region are very sensitive to the position at which the interaction occurs; they are thus subject to considerable error because the position of interaction is rather unsteady owing to flow turbulence and its repeatability, although good, is not perfect. Furthermore, the presence of the hot-wire probe was found to produce some change in the static pressure distribution on the wall in the interaction region. To minimize these interference effects a hot-wire probe having particularly small prong and stem diameters (TSI model 1275-T 1·5) was used to take the measurements for figures 7(*a*) and (*b*).

Measurements in the two-dimensional free jet that forms as a result of the interaction were rather difficult because the position and direction of the jet fluctuated considerably and because the turbulence level was high. The few measurements that were taken produced no evidence of a velocity minimum in the flow; in fact the results (plotted in figure 8) show that at a distance of less than $2(y_{\frac{1}{2}m1i}+y_{\frac{1}{2}m2i})$ from the wall the observed velocity profile is already in good agreement with Forthmann's (1934, see Schlichting 1960) measurements in a two-dimensional free jet. This rapid response of the flow is undoubtedly due to the high turbulence level. Figure 9 compares measurements of the longitudinal turbulence in the present free jet with those of Bradbury (1965) in a conventionally generated two-dimensional free jet in still air. The turbulence level in the present jet is seen to be roughly three times as large as that in Bradbury's jet.

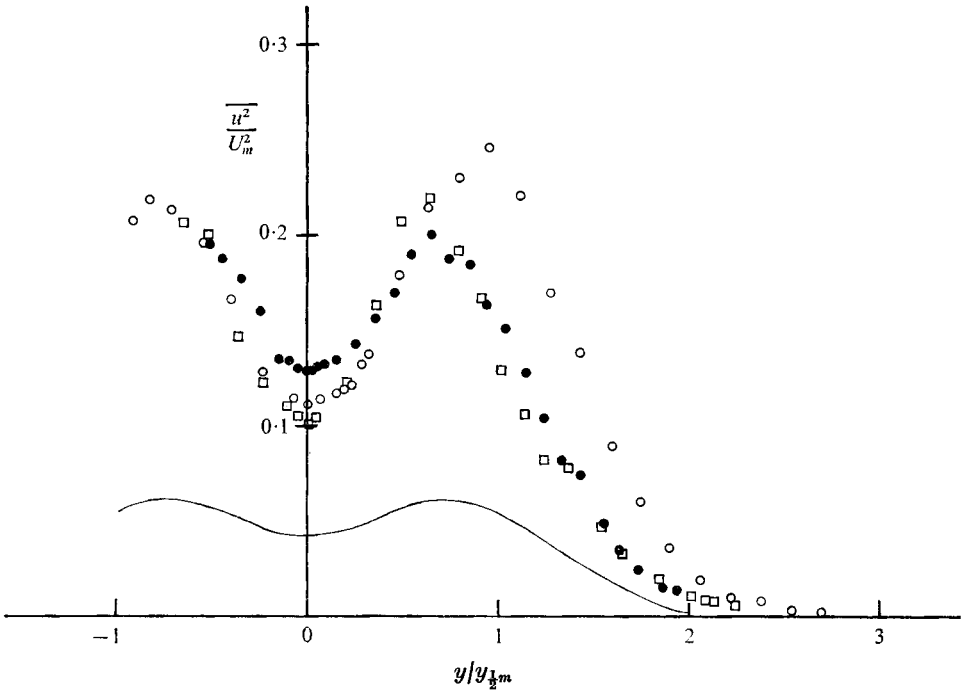

FIGURE 9. Longitudinal turbulence in free jet after interaction. ——, mean line through data of Bradbury (1965) for a two-dimensional free jet. For other symbols see figure 8.

The rate of spread of the present free jet was likewise found to be about three times as large as that of a conventionally generated free jet.

The flow in the interaction region was observed to be highly unsteady in a statistical sense. This fact and the fact that the mixing is non-parallel might lead one to expect that appreciable mixing losses could occur during the interaction; that is, that the resultant momentum flux of the jet after the interaction could be less than the sum $|J_1'| + |J_2'|$ of the individual wall-jet momentum fluxes. For example, if two turbulent free jets directed at 90° to one another and of equal momentum flux J are made to interact, the resultant momentum flux in real flow is only $J\sqrt{2}$, implying a momentum loss of $(2-\sqrt{2})J$. However, the experiments showed that there is little, if any, such loss in the present flow. The momentum of the free jet was determined in two different ways: first, by integration of the free-jet velocity profiles, and second, by integration of the static-pressure distributions along the wall and use of the momentum theorem. Within the experimental error (which was about $\pm 10\,\%$ of J) there appears to be no loss of momentum in the interaction process. Given this result, it is easy to predict the angle of the free jet after the interaction from momentum considerations.

In the common beam-deflexion fluidic proportional amplifier a power jet of momentum flux J_1 is deflected through some angle θ by a control jet of momentum flux J_2; the control jet is approximately normal to the power jet and the interaction takes place in free air so that, for small J_2/J_1,

$$\theta \doteq J_2/J_1. \tag{14}$$

Returning now to the wall-jet interaction described in this paper, let us consider wall jet 1 as the power jet and wall jet 2 as the control jet; from the results of the preceding paragraph, the angle θ of the jet leaving the interaction will be given by

$$\theta = \cos^{-1}\left(\frac{J_1 - J_2}{J_1 + J_2}\right) \doteqdot 2\left(\frac{J_2}{J_1}\right)^{\frac{1}{2}}. \tag{15}$$

For small values of J_2/J_1 the right-hand side of (15) is several times larger than that of (14). The gain of a fluidic amplifier based on the wall-jet interaction process is thus potentially much larger than that of the beam-deflexion amplifier. Moreover the gain of the wall-jet interaction amplifier would be further enhanced by the fact that the position of the interaction depends on the value of J_2/J_1. Unfortunately, (15) is nonlinear; this deficiency could probably, however, be overcome by using a suitably curved wall between the two blowing slots. The unsteadiness and high turbulence level of the jet leaving the interaction would result in a poor signal-to-noise ratio for an amplifier based on the wall-jet interaction phenomenon.

4. A physical explanation for some of the experimental results

Equations (12) and (13) indicate that the separation processes are dynamically similar for all values of J_1/J_2 and for both the weak and strong wall jets. This result is somewhat surprising since in the unequal interactions the geometry of the flow, at least after separation, is quite different on the weak-jet and strong-jet sides of the flow. A simple explanation of the observed result can, however, be formulated on the basis of the 'frozen-flow' concept of Stratford (1959) and Townsend (1961). According to this concept the total head remains essentially constant along streamlines in the outer region of a turbulent boundary layer approaching separation because the adverse pressure gradient is large compared with the shear stress gradient. Figure 5 shows that the pressure rise up to separation is very rapid† in the present flow so that the frozen-flow assumption should apply over most of the inner layer ($y < y_m$) of the wall jet during this pressure rise. The inner-layer velocity profile at the start of the pressure rise (position A) can be described by some profile equation, say

$$\frac{U_A}{U_{mA}} = f_A\left[\frac{y}{y_m}\right]_A. \tag{16}$$

By applying Bernoulli's equation along the streamline through $y = y_{mA}$ and along another streamline with ordinate y in the inner layer one can obtain the relation

$$\left(\frac{U_B}{U_{mB}}\right)^2 = \frac{(f_A[y/y_m]_A)^2 - \Delta C_p}{1 - \Delta C_p}, \tag{17}$$

where $\Delta C_p \equiv (p_B - p_\infty)/\frac{1}{2}\rho U_{mA}^2$ and subscript B denotes a position downstream of position A. In deriving (17) it has been assumed that $\partial p/\partial y = 0$ for $0 < y < y_m$. Equation (17) shows that

$$\frac{U_B}{U_{mB}} = f\left[f_A\left[\frac{y}{y_m}\right]_A, \frac{p_B - p_\infty}{\frac{1}{2}\rho U_{mA}^2}\right]. \tag{18}$$

† Ninety per cent of the overall pressure rise occurs over a streamwise distance of about $10y_m$, where y_m is the height at which the velocity in the wall jet has its maximum value.

Thus for a given initial profile shape $f_A[y/y_m]$ the downstream profile shapes $(U_B/U_{mB})\,[y/y_m]$ will be identical if the pressure-rise coefficients ΔC_p are identical. Now in the wall-jet interaction process the initial profile shape and the pressure rise $p_B - p_\infty$ to separation are in fact the same for both wall jets; therefore, by (18), both wall jets must have the same maximum velocity U_{mA} at the start of the pressure rise if the inner-layer shape parameter at separation is to be the same for both wall jets, as one would expect it to be. If one assumes that the inner-layer shape parameter at separation has a unique value for all cases and that the inner-layer profile shape is the same for all zero-pressure-gradient wall jets (i.e. f_A is fixed) then one can also conclude from (18) that $(p_{\text{sep}} - p_\infty)/\frac{1}{2}\rho U_{mA}^2$ must have a unique value for all cases. These two conclusions can be shown to be in agreement with (8) and (12) by using the facts that, approximately, U_m^2 is proportional to J/x for still-air wall jets and that the distance between the start of the pressure rise and the position of interaction is proportional to the wall-jet thickness and hence to x. Since (8) originally followed from (4), the frozen-flow concept also predicts (4).

It has already been pointed out that at a given pressure coefficient the velocity and turbulence profiles of figures 7 (*a*) and (*b*) are the same in the inner layer of both the weak and the strong wall jets. This finding supports the applicability of the frozen-flow concept since it is exactly what (18) suggests should occur.

A tempting alternative explanation of the results would be adoption of the hypothesis that the wall jets impact and stagnate in the interaction region so that the maximum static pressure is approximately equal to the maximum dynamic pressure, $\frac{1}{2}\rho U_m^2$, of the wall jets. Equation (8) then follows immediately since the stagnation pressures of both wall jets would have to be the same at the impact position. Use of (2), ignoring the small constant term, then easily leads to (3) and (4), with a value of 16 for the constant on the right-hand side of (3). Indeed a more accurate derivation of (3), by use of (11), gives a value of 12·5 for the right-hand side of (3); this is only 25 % high and of course the constant on the right-hand side of (12) is assumed to be about 1, only 20 % too high. Nevertheless, it is felt that this explanation is incorrect. The results of the surface flow visualization and the static-pressure distributions of figure 5 both indicate that the flow behaves essentially as sketched in figure 1; that is, that there is no stagnation point in the flow other than perhaps in the nearly 'dead' air in the separation bubble. Although the pressure terms almost certainly dominate the turbulent stress terms in the equations of motion, the stagnation pressure is far from uniform across the wall jets and the flow is bounded by a wall, so that one cannot expect a stagnation point as is found in the classical potential-flow solution for impacting jets. Rather, in the present flow, the strong adverse pressure gradient causes the boundary-layer-like flow to separate from the wall and the high static pressure in the interaction region is due to the curvature of the flow leaving the wall, not to any stagnation of the flow.

The results of a simple experiment provide further evidence that the correct explanation of the results is that based on the frozen-flow concept. A strip of tape (0·43t thick by 3t wide) was fixed to the wall with its leading edge 81t downstream of slot 2. This is approximately where the static pressure would begin to

rise in the case of an equal interaction with no obstruction. In fact, with $J_1/J_2 = 1{\cdot}0$ the position of interaction was shifted a distance of $24t$ towards the tape from its usual position at the centre of the apparatus. Measurements showed that the tape caused a decrease of only 3 % in the maximum velocity U_{m2} at the position of interaction and the momentum J_2 was unaffected as evidenced by the fact that the resultant jet leaving the interaction remained vertical. In summary, with the tape in place the results were as follows:

$$(J_1/J_2)_i = 1{\cdot}0; \quad (x_1/x_2)_i = 1{\cdot}5; \quad (U_{m1}/U_{m2})_i = 0{\cdot}82;$$
$$(p_{\text{sep}} - p_\infty)/\tfrac{1}{2}\rho U_{m1i}^2 = 0{\cdot}8; \quad \text{and} \quad (p_{\text{sep}} - p_\infty)/\tfrac{1}{2}\rho U_{m2i}^2 = 0{\cdot}55.$$

These results cannot be explained by assuming that the wall jets stagnate during the interaction process; they are, however, perfectly compatible with the explanation based on the frozen-flow concept since the tape of course distorts the velocity profile in the inner layer of wall jet 2 such that it is prone to earlier separation.

5. Conclusions

The interaction occurs at a position such that $x_{1i}/J_1 = x_{2i}/J_2$ and at the position of interaction the maximum velocity U_{mi} is equal for both wall jets regardless of the value of J_1/J_2. The separation-pressure coefficient $(p_{\text{sep}} - p_\infty)/\tfrac{1}{2}\rho U_{mi}^2$ has a unique value of about 0·8 for all cases. These results can be explained on the basis of the 'frozen-flow' concept.

The free jet that results from the interaction acquires the same time-average velocity distribution as a conventionally generated free jet with remarkable rapidity, but its turbulence level and rate of spread are about three times larger. There appears to be no loss of momentum in the interaction process. The flow holds some promise as the basis of a fluidic proportional amplifier.

The authors are grateful for the financial support provided by the National Research Council of Canada through operating grant number A-5173.

REFERENCES

BRADBURY, L. J. S. 1965 *J. Fluid Mech.* **23**, 31.
GARTSHORE, I. S. & NEWMAN, B. G. 1969 *Aero. Quart.* **20**, 25.
GILES, J. A., HAYS, A. P. & SAWYER, R. A. 1965 *Aero. Quart.* **17**, 201.
KIND, R. J. 1967 Ph.D. dissertation, University of Cambridge.
KIND, R. J. 1971 *Can. Aero. & Space Inst. Trans.* **4**, 2.
KIND, R. J. & MAULL, D. J. 1968 *Aero. Quart.* **19**, 170.
KRUKA, V. & ESKINAZI, S. 1964 *J. Fluid Mech.* **20**, 555.
MYERS, G. E., SCHAUER, J. J. & EUSTIS, R. N. 1963 *J. Basic Eng.* **85**, 47.
SCHLICHTING, H. 1960 *Boundary Layer Theory*, 4th edn., p. 207. McGraw-Hill.
STRATFORD, B. S. 1959 *J. Fluid Mech.* **5**, 1.
TOWNSEND, A. A. 1961 *J. Fluid Mech.* **12**, 536.